Journal of Photochemistry and Photobiology A: Chemistry 225 (2011) 42–51

Contents lists available at SciVerse ScienceDirect

Journal of Photochemistry and Photobiology A: Chemistry

journal homepage: www.elsevier.com/locate/jphotochem

Thermal protein unfolding in photo-activated adenylate cyclase nano-clusters from the amoeboflagellate *Naegleria gruberi* NEG-M strain

A. Penzkofer[a,*], M. Stierl[b], P. Hegemann[b], S. Kateriya[c]

[a] Fakultät für Physik, Universität Regensburg, Universitätsstrasse 31, D-93053 Regensburg, Germany
[b] Institut für Biologie/Experimentelle Biophysik, Humboldt Universität zu Berlin, Invalidenstrasse 42, D-10115 Berlin, Germany
[c] Department of Biochemistry, University of Delhi South Campus, Benito Juarez Road, New Delhi 110021, India

ARTICLE INFO

Article history:
Received 12 July 2011
Received in revised form
17 September 2011
Accepted 24 September 2011
Available online 1 October 2011

Keywords:
Photo-activated adenylate cyclase (PAC)
BLUF domain
Amoeboflagellate *Naegleria gruberi*
Flavin
Protein unfolding
Apparent protein melting temperature
Protein melting time
Protein melting enthalpy
Protein melting entropy
Light attenuation
Light scattering
Fluorescence behavior
Measurement standard of protein melting temperature

ABSTRACT

The photo-activated adenylate cyclase (nPAC) protein from the amoeboflagellate *Naegleria gruberi* NEG-M strain consists of a BLUF domain (sensor of blue light using flavin) and a cyclase homology domain (CHD). The nPAC thermal stability is determined by its protein unfolding behavior which is quantified by the protein melting temperature and protein melting time. The protein unfolding in nPAC nano-clusters in aqueous solution at pH 7.5 is studied by light attenuation and fluorescence measurements. The temporal behavior of protein unfolding (denaturation) is monitored by observation of spectral changes of the first absorption band of the flavin cofactor. The nPAC unfolding occurs irreversible in a bi-exponential manner (different melting time constants for proteins at nano-cluster surface and in nano-cluster interior). The nPAC apparent melting temperature (there half of the proteins are unfolded) is determined by light attenuation measurement (light scattering increases due to coalescing of unfolded protein nano-clusters) in the non-absorbing spectral region of the protein. A measurement standard is developed employing a staircase temperature heating and cooling profile. High thermal stability of nPAC nano-clusters in pH 7.5 aqueous solution was found with an apparent melting temperature of 60 °C.

1. Introduction

Naegleria gruberi is a widespread free-living soil and freshwater amoeboflagellate [1–4]. Different strains of *N. gruberi* exist in the nature. Recently, the genome sequence of the *N. gruberi* NEG-M strain (ATCC 30224) [2] was determined and most of the genes were annotated [5]. This amoeboflagellate contains at least 108 cyclase genes. Four of them occur in combination with BLUF domains [5] (BLUF = sensor of blue-light using flavin) making them to putative photo-activated cyclases (PACs) which catalyze light-controlled chemical reactions to form cyclic compounds. One of these PACs, the soluble photo-activated adenylate cyclase nPAC (nPAC = *Naegleria* photo-activated cyclase, GenBank accession XP_002674372 and JF928492) causes blue-light regulated cyclic adenylyl monophosphate formation (cAMP) from adenosine triphosphate (ATP) [6]. The expression and purification of nPAC are described in [7]. The photo-cycle dynamics of the BLUF domain of nPAC in aqueous pH 7.5 phosphate buffer solution is presented in detail in [7]. At room temperature nPAC in pH 7.5 buffer was found to be aggregated to nano-crystallites/nano-clusters (oligomeric form) with color-center emission besides the fluorescence from the flavin cofactor and the intrinsic fluorescence from tyrosine and tryptophan residues [8].

Here the protein unfolding (denaturation) of nPAC is studied in detail. The investigations were undertaken (i) to get information on the thermal stability of this blue-light sensitive cyclase, (ii) to study experimentally and theoretically the thermal unfolding of proteins especially of irreversible denaturating proteins, and (iii) to develop a measurement standard for the determination of the apparent melting temperature of irreversible denaturating proteins.

Thermal stability investigations on proteins are reviewed in [9–13]. Regarding protein thermal stability characterization with melting temperature and melting time determination one has to

* Corresponding author. Tel.: +49 941 943 2107; fax: +49 941 943 2754.
E-mail address: alfons.penzkofer@physik.uni-regensburg.de (A. Penzkofer).

1010-6030/$ – see front matter © 2011 Elsevier B.V. All rights reserved.
doi:10.1016/j.jphotochem.2011.09.024

distinguish between irreversible unfolding proteins and reversible unfolding proteins:

(i) For irreversible protein unfolding the amount of unfolded protein is time and temperature dependent. The melting temperature, ϑ_m, where half of the proteins are unfolded depends on the applied heating profile. One speaks of apparent melting temperature to remind of its dependence on the measurement procedure. The protein melting half-time, t_m, (duration needed to unfold half of the initially folded proteins) is well defined at a fixed temperature. The temporal unfolding relation is given by $N(t) = N(0)\exp[-\ln(2)t/t_m]$ where $N(t)$ and $N(0)$ are the number densities of folded proteins at times t and 0. t_m shortens with increasing temperature in an Arrhenius-type manner.

(ii) For reversible protein unfolding and refolding, there exists a thermodynamic equilibrium between the folded und unfolded protein states. The protein melting temperature, ϑ_m, is thermodynamic well defined as the temperature where under steady-state conditions the number density N of native folded proteins is equal to the number density U of unfolded proteins, i.e. fraction of folded proteins, $f_f = N/N_0 = 0.5$ and fraction of unfolded proteins, $f_{un} = U/N_0 = 0.5$ ($N_0 = N + U$ is total protein number density) [14–16]. At the melting temperature ϑ_m – after equilibration – the rate of protein unfolding is equal to the rate of protein refolding. The equilibrium formation time, τ_m, at a fixed temperature is defined according to the relation

$$N(t) - N_{eq} = [N(0) - N_{eq}]\ \exp\left(\frac{-t}{\tau_m}\right)$$

where N_{eq} is the number density of unfolded proteins at equilibrium. τ_m depends on the specific protein and decreases with rising temperature.

Reversible thermal unfolding and refolding of proteins were observed for small proteins in [9,17]. It was observed for the globular proteins bovine serum albumin, RNAase and catalase within a certain range of pH [18], and for the hyperthermophile protein Sac7d from *Sulfolobus acidocaldarius* in a pH range from 0 to 10 [19]. Reversible unfolding and refolding of proteins at a fixed temperature are often achieved with chemical denaturants like urea or guanidinium chloride [10,20–22]. For refolding the denaturant concentration may be decreased by dialyses or dilution.

The thermal protein denaturation is mostly irreversible because of strong tendency of unfolded proteins to aggregate, chemically react, or degrade [9,23]. In the case of irreversible protein denaturation, there is no existence of thermodynamic equilibrium between folded and unfolded state. There is only a thermo-kinetic process of protein unfolding.

The nPAC protein unfolding showed up in strong increase of light-scattering, in loss of the vibronic structure of the flavin cofactor S_0–S_1 absorption band, in a rise of the flavin fluorescence, and in a decrease of the native protein (tyrosine, tryptophan) fluorescence. The nPAC protein unfolding was found to be irreversible.

The protein unfolding (both reversible and irreversible) may be studied and the protein melting temperature (reversible situation) or the apparent melting temperature (irreversible situation) may be determined by any process which changes in the changeover from the native folded protein form to the denatured unfolded form. Applied techniques for studying protein folding and unfolding are temperature dependent measurements of the circular dichroism [16,17,24], the optical rotation [25,26], the ultraviolet absorption [25,27], the fluorescence [15,28], the dynamic light scattering [29], the static light scattering [30,31], and the viscosity [25], or the use of differential scanning calorimetry [17,28,32,33].

Theoretical considerations of reversible protein folding [15,16,34–36], partial reversible and irreversible protein melting [15,28,36], and irreversible protein unfolding [16,36] have been undertaken. Theoretical predictions of the protein melting temperature from the amino acid sequence have been reported [37–39]. The denatured protein may be thermodynamically described as a random coil [40], while detailed spectroscopic inspection reveals the remaining of local amino acid residue–amino acid residue interaction and some remaining sub-structure [40–45].

Here we determine the apparent nPAC melting temperature from light attenuation measurements for an applied temporal temperature staircase profile. The applied measurement routine is proposed as a standard for measuring the apparent melting temperature of irreversible unfolding proteins.

The time dependence of the nPAC protein unfolding on the sample temperature, ϑ, is studied by measuring temporal absorption spectra changes of the S_0–S_1 absorption band of the flavin cofactor (loss of vibrational structure of absorption band with flavin release from binding pocket).

2. Materials and methods

The heterologous expression of nPAC in *Escherichia coli* was described previously [7]. The nPAC protein comprises a BLUF domain (consisting of 94 amino acids) with a flavin molecule as cofactor (composition: 70% flavin mononucleotide FMN, 30% flavin adenine dinucleotide FAD) and of a cyclase homology domain (CHD consisting of 177 amino acids). The total number of amino acids of the protein is 390. The molar mass of the apo-protein is $M_{pr} = 43\,962\ g\,mol^{-1}$ (see GenBank XP_002674372 and JF928492). The nPAC protein was dissolved in pH 7.5 aqueous buffer consisting of 10 mM NaH_2PO_4/Na_2HPO_4 and 10 mM NaCl. The nPAC number density of the samples used for the measurements was $N_0 \approx 4.3 \times 10^{16}\ cm^{-3}$ (concentration $C_0 \approx 7.1 \times 10^{-5}\ mol\,dm^{-3}$). The samples were stored at −80 °C after expression until measurements.

Transmission measurements were carried out with a spectrophotometer (Cary50 from Varian). For the determination of the apparent melting temperature a temperature controlled absorption cell (type 165-QS from Hellma, Müllheim, Germany, light path 1 mm, volume 160 μl) connected to a thermostatic water bath with external circulation was used in the spectrophotometer. The applied temporal staircase temperature profile in the transmission measurements is shown below in Fig. 2a. For the temporal protein unfolding studies at fixed temperatures an ultra-micro-cell (type 105-QS from Hellma, width 1.5 mm, length 3 mm, height 5 mm, fill volume 20 μl) was set in the thermostatic water bath, and it was periodically taken out for transmission measurements.

Attenuation coefficient spectra, $\alpha(\lambda, \vartheta)$ and cross-section spectra, $\sigma(\lambda, \vartheta)$ (λ is wavelength and ϑ is temperature), were calculated from the measured transmission spectra, $T(\lambda, \vartheta)$, by the relations $\alpha(\lambda, \vartheta) = -\ln[T(\lambda, \vartheta)]/\ell$ and $\sigma(\lambda, \vartheta) = \alpha(\lambda, \vartheta)/N_0$, where ℓ is the sample length and N_0 is the total nPAC number density. The attenuation coefficient α (attenuation cross-section σ) is composed of the absorption coefficient α_a (absorption cross-section σ_a) and the scattering coefficient α_{sca} (scattering cross-section σ_{sca}) according to $\alpha = \alpha_a + \alpha_{sca}$ ($\sigma = \sigma_a + \sigma_{sca}$). The scattering coefficient (cross-section) increases with the transfer from the folded protein state to the unfolded protein state if the protein unfolding is accompanied with protein aggregation. The increase of light attenuation will be used below to determine the apparent melting temperature of nPAC. The absorption strength, $\bar{\sigma}_a = \int[\sigma_a(\lambda)/\lambda]\,d\lambda$, remains approximately unchanged in the process of protein denaturation. The shapes of the flavin and apo-protein absorption spectra change slightly with the protein unfolding. Especially the vibronic

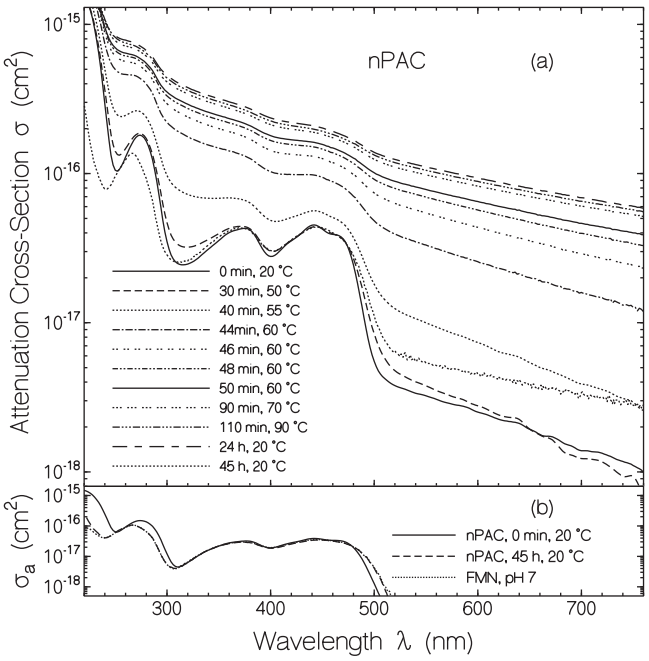

Fig. 1. (a) Attenuation cross-section spectra development, $\sigma(\lambda)$, of nPAC during thermal denaturation process. Applied heating profile is shown in Fig. 2a. Measurement time positions and temperatures are given in legend. (b) Absorption cross-section spectra, $\sigma_a(\lambda)$, of native nPAC (solid curve) and of denatured nPAC (dashed curve). For comparison, the absorption cross-section spectrum of FMN in aqueous solution at pH 7 is included (from [52]).

structure of the S_0–S_1 absorption band of flavin is smeared out in the unfolded state. The loss of vibronic absorption structure will be used below to study the temporal development of the protein unfolding at selected sample temperatures.

Fluorescence emission spectra and fluorescence excitation spectra were recorded with a fluorimeter (Cary Eclipse from Varian) before and after thermal protein denaturation. Magic angle conditions were applied for the fluorescence recording (vertical polarized excitation, and orientation of the fluorescence detection polarizer at an angle of 54.7° to the vertical [46]). The spectra were corrected for the spectral sensitivity of the spectrometer and the photo-detector [47,48].

3. Results

3.1. Apparent melting temperature determination

Attenuation cross-section spectra, $\sigma(\lambda)$, of nPAC measured at different temperatures and times are shown in Fig. 1a. The applied temporal staircase temperature profile is depicted in Fig. 2a. In the wavelength range $\lambda > 520$ nm absorption is negligible and the attenuation is solely determined by light scattering. In the wavelength region from 520 nm to 320 nm the absorption is caused by flavin cofactor excitation. For $\lambda < 320$ nm the amino acids, mainly tryptophan (1 Trp per protein) and tyrosine (11 Tyr per protein), and the flavin cofactor contribute to the absorption.

For a freshly thawed nPAC sample (time $t = 0$, thin solid curve in Fig. 1a) at room temperature a weak Rayleigh light scattering is already present (e.g. $\sigma_{sca}(632\,\text{nm}) = 2.16 \times 10^{-18}\,\text{cm}^2$) since nPAC does not thaw to monomers but forms nano-clusters (aggregates/nano-crystallites) [8]. The vibronic structure of the first absorption band of flavin ($400\,\text{nm} < \lambda < 500\,\text{nm}$) is indicative of holding the flavin in the BLUF domain binding pocket [7]. Heating up to 50 °C in a time period of 30 min did not change appreciably the attenuation spectrum (dashed curve in Fig. 1a, only slight increase in scattering, no change of vibronic structure of flavin S_0–S_1 absorption). The thin dotted curve in Fig. 1a belonging to $\vartheta = 55\,^\circ\text{C}$ and $t = 40$ min shows already an appreciable increase of light scattering (e.g. $\sigma_{sca}(632\,\text{nm}) = 6.05 \times 10^{-18}\,\text{cm}^2$) and reduced vibronic structure of the first flavin absorption band. Increasing the temperature to 60 °C caused a steep rise of light scattering (e.g. $\sigma_{sca}(632\,\text{nm},\ 44\,\text{min}) = 2.19 \times 10^{-17}\,\text{cm}^2$, $\sigma_{sca}(632\,\text{nm},\ 46\,\text{min}) = 3.81 \times 10^{-17}\,\text{cm}^2$, $\sigma_{sca}(632\,\text{nm},\ 48\,\text{min}) = 5.05 \times 10^{-17}\,\text{cm}^2$, $\sigma_{sca}(632\,\text{nm},\ 50\,\text{min}) = 5.81 \times 10^{-17}\,\text{cm}^2$) and a smoothening of the first flavin absorption band. The increase in scattering shows a growth of protein aggregation. The wavelength dependence of scattering is approximately given by $\sigma_{sca}(\lambda) = \sigma_{sca}(\lambda_0)(\lambda_0/\lambda)^\gamma$ with $\gamma = 4$ for Rayleigh scattering and $\gamma < 4$ for Mie scattering whereby γ decreases with aggregate radius growth [49–51]. A smoothening of the first flavin absorption band occurred due to cofactor release from the BLUF domain binding pocket. Further increase of the temperature caused a moderate increase of light scattering (e.g. $\sigma_{sca}(632\,\text{nm},\ 90\,\text{min},\ 70\,^\circ\text{C}) = 7.44 \times 10^{-17}\,\text{cm}^2$, $\sigma_{sca}(632\,\text{nm},\ 110\,\text{min},\ 90\,^\circ\text{C}) = 7.98 \times 10^{-17}\,\text{cm}^2$) indicating a moderate growth of aggregation. Cooling down of the sample did not reduce the light scattering showing that the protein denaturation occurred irreversibly (e.g. after 24 h was $\sigma_{sca}(632\,\text{nm},\ 20\,^\circ\text{C}) = 8.42 \times 10^{-17}\,\text{cm}^2$, thick dash-dotted curve in Fig. 1a).

After 26 h the nPAC sample was transferred to a fused silica ultra-micro cell (type 105-QS from Hellma) for fluorescence measurements. This transfer initiated apo-protein sedimentation. Within about 3 h light attenuation due to scattering strongly decreased. The thick dotted curve in Fig. 1a shows the attenuation coefficient spectrum at $t = 45$ h (42 h after heat treatment, $\sigma(632\,\text{nm},\ 45\,\text{h},\ 20\,^\circ\text{C}) \approx 4.19 \times 10^{-18}\,\text{cm}^2$).

The extracted absorption cross-section spectra, $\sigma_a(\lambda)$, of nPAC before heat treatment ($t = 0$, solid curve) and after denaturation ($t = 45$ h, dashed curve) are shown in Fig. 1b (scattering contributions from curves in Fig. 1a are subtracted). For comparison the absorption cross-section spectrum of FMN (flavin mononucleotide) in aqueous pH 7 solution is also shown (dotted curve, taken from [52]). The long-wavelength-absorption tail of flavin in native nPAC decreases steeper than the absorption tail of released flavin after denaturation or of FMN in aqueous solution. For $\lambda < 320$ nm the apo-protein absorption contribution of native nPAC is clearly seen. For the denatured nPAC ($t = 45$ h) the apo-protein absorption is no longer present because of apo-protein sedimentation.

The temporal development of the light scattering due to sample heating and cooling at the fixed wavelength of $\lambda = 700$ nm is shown in Fig. 2. In part (a) the applied temporal temperature profile $\vartheta(t)$ is depicted, part (b) shows the measured attenuation cross-sections $\sigma(700\,\text{nm},\ t)$, and part (c) shows the attenuation cross-section derivative $\partial\sigma_{sca}(700\,\text{nm},\ t)/\partial t$. The sample was heated up in steps to 60 °C where a strong rise in light scattering occurred due to aggregation of unfolded (melted) protein. Then the temperature was decreased to 55 °C to check the reversibility. It turned out that the light scattering (aggregation) continued to increase slightly, which showed that the unfolding of nPAC was an irreversible process. Following, the temperature was increased stepwise to 90 °C. Thereby the light-scattering continued to increase moderately due to moderate cluster growth by aggregation. During the next stepwise cooling down to room temperature the light scattering still increased slightly. The light attenuation behavior at 20 °C was observed over a period of 20 h (data not shown). In this time period the light attenuation remained unchanged. The change of the light-scattering versus time, $\partial\sigma_{sca}(700\,\text{nm},\ t)/\partial t$, for the applied temperature profile of Fig. 2a shows a peak at $t = 45$ min where $\vartheta = 60\,^\circ\text{C}$. This temperature is the apparent melting temperature ϑ_m of nPAC for the applied heating profile. It should be noticed

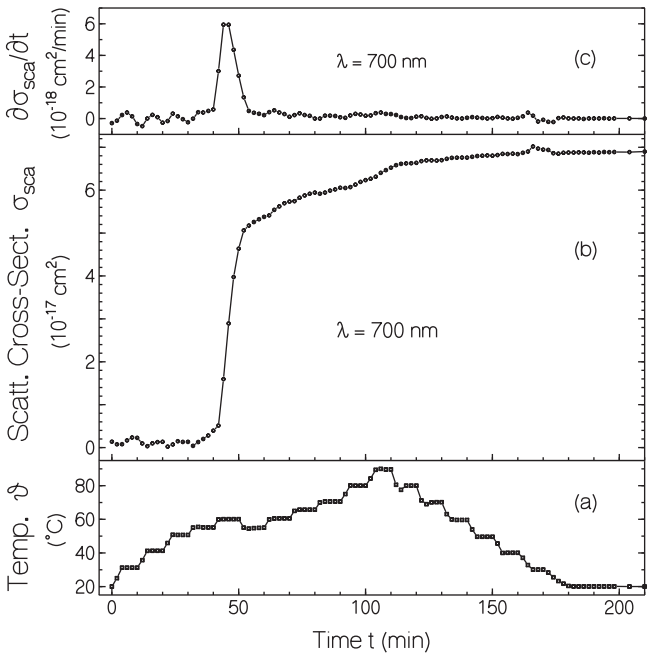

Fig. 2. (a) Applied heating and cooling staircase profile in nPAC denaturation process. (b) Temporal development of scattering cross-section at 700 nm in the nPAC denaturation process. (c) Time derivative, $\partial\sigma_{sca}(700\,nm)/\partial t$ of scattering cross-section in nPAC denaturation process.

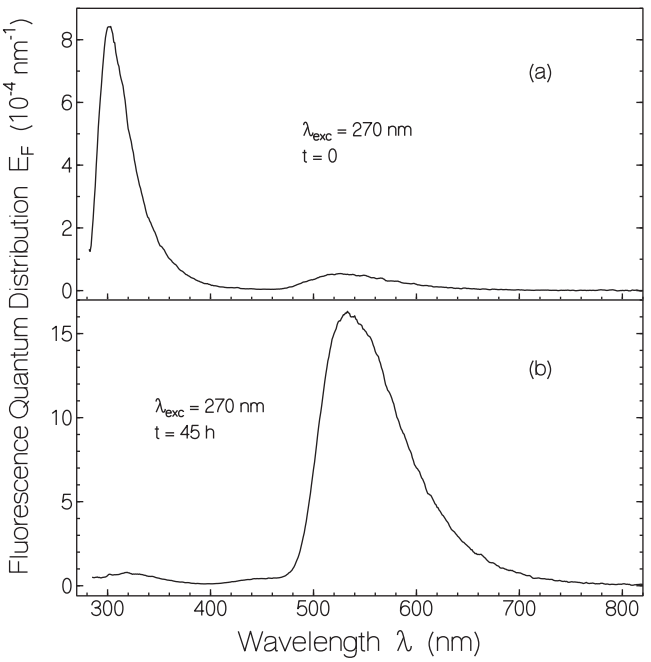

Fig. 4. Fluorescence quantum distributions, $E_F(\lambda)$, of nPAC before denaturation (a) and after denaturation (b) for fluorescence excitation at $\lambda_{exc} = 270$ nm.

that the temperature ϑ_m associated with the maximum of $\partial\sigma_{sca}/\partial t$ depends on the shape of the applied temperature profile (maximum of $\partial\sigma_{sca}/\partial t$ would occur at lower temperature for slower heating up).

The scattering cross-section, $\sigma_{sca}(700\,nm)$, versus sample temperature for the applied temporal temperature profile of Fig. 2a is depicted in Fig. 3. The main protein unfolding in the time interval from 42 min to 50 min at $\vartheta = 60\,^{\circ}C$ is clearly seen. During cooling down of the nPAC sample the light scattering did not decrease

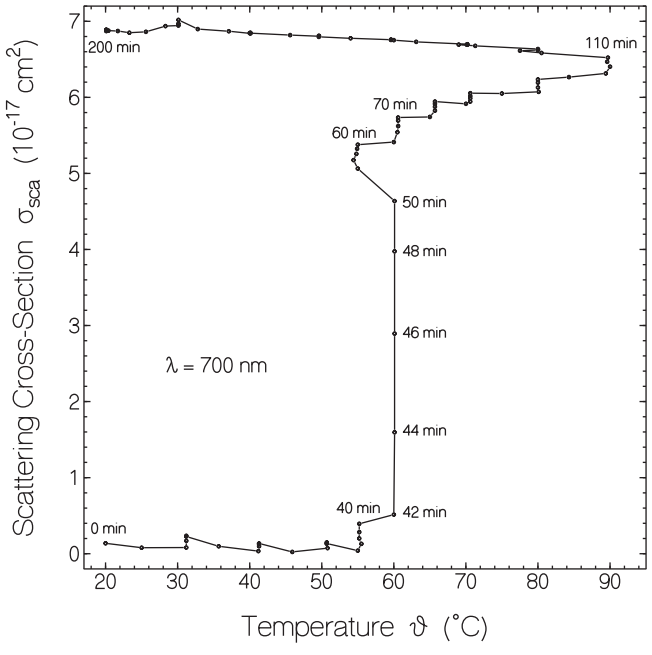

Fig. 3. Plot of scattering cross-section $\sigma_{sca}(700\,nm)$ of nPAC versus temperature of applied temperature profile of Fig. 2a.

showing the irreversible unfolding of nPAC in the heating process (no decrease of degree of aggregation in the cooling process).

The fluorescence emission behavior of nPAC is shown in Fig. 4. The fluorescence quantum distribution $E_F(\lambda)$ is depicted, which is defined as the ratio of the total intrinsic spectral density of emitted photons, $dn_{ph,em}(\lambda)/d\lambda$, to the total number of absorbed photons, $n_{ph,abs}$, at the excitation wavelength λ_{exc} [47,53,54]. The fluorescence excitation occurred at $\lambda_{exc} = 270$ nm.

In Fig. 4a $E_F(\lambda)$ of native nPAC is shown before heat treatment ($t = 0$). The corresponding fluorescence quantum yield, $\phi_F = \int E_F(\lambda)\,d\lambda$, is $\phi_F(t=0) \approx 0.042$ with a contribution of 0.0365 from the apo-protein (mainly Tyr) and a contribution of 0.0055 from the flavin.

In Fig. 4b $E_F(\lambda)$ of denatured nPAC is shown at time $t = 45$ h. The total fluorescence quantum yield increased to $\phi_F \approx 0.173$. The apo-protein fluorescence contribution decreased strongly to $\phi_{F,apo\text{-}protein} \approx 0.005$ due to apo-protein sedimentation out of the excitation and detection volume. The fluorescence maximum of the denatured nPAC apo-protein occurred at $\lambda \approx 319$ nm. A small fluorescence contribution from lumichrome is observed (emission in region 400 nm to 470 nm, quantum yield contribution $\phi_{F,lumichrome} \approx 0.002$). It was formed by the heat treatment. The dominant fluorescence quantum yield contribution of $\phi_{F,flavin} \approx 0.165$ comes from the flavin released from the BLUF domain binding pocket. The flavin composition in native nPAC was 70% FMN and 30% FAD (flavin adenine dinucleotide). The fluorescence quantum yields of FMN and FAD in neutral aqueous solution are $\phi_F(FMN) \approx 0.23$ [52] and $\phi_F(FAD) \approx 0.033$ [55].

Normalized fluorescence excitation spectra, $E'_{ex}(\lambda)$, [48] of native nPAC ($t = 0$) and denatured nPAC ($t = 35$ h) are shown in Fig. 5a and b, respectively. For native nPAC (Fig. 5a) fluorescence detection at $\lambda_{det} = 540$ nm, 345 nm, and 310 nm resulted in the fluorescence excitation quantum distributions of flavin, tryptophan, and tyrosine, respectively. For denatured nPAC (Fig. 5b) fluorescence detection at $\lambda_{det} = 540$ nm gave the fluorescence excitation quantum distribution of released flavin in the aqueous pH 7.5 buffer solution. Fluorescence detection at 440 nm revealed the fluorescence excitation quantum distribution of lumichrome [56]. The

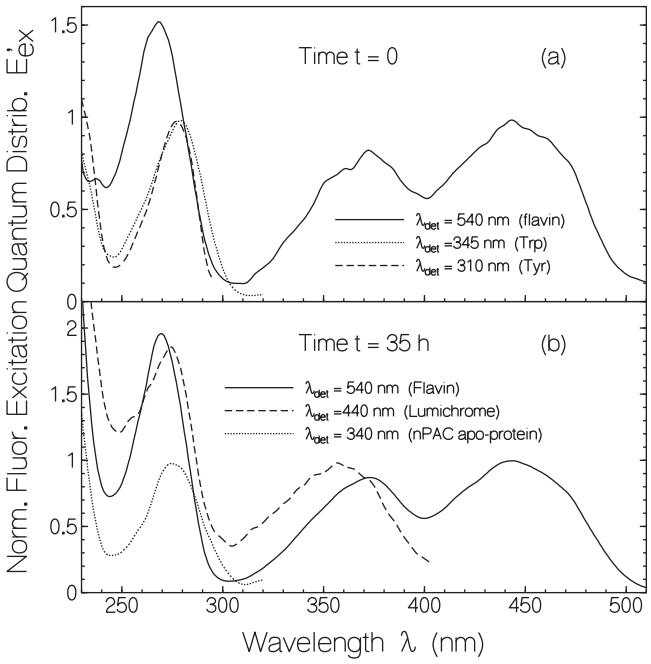

Fig. 5. Fluorescence excitation spectra, $E'_{ex}(\lambda)$, of nPAC at selected fluorescence detection wavelengths, λ_{det}, before denaturation (a) and after denaturation (b). Applied heating profile is shown in Fig. 2a.

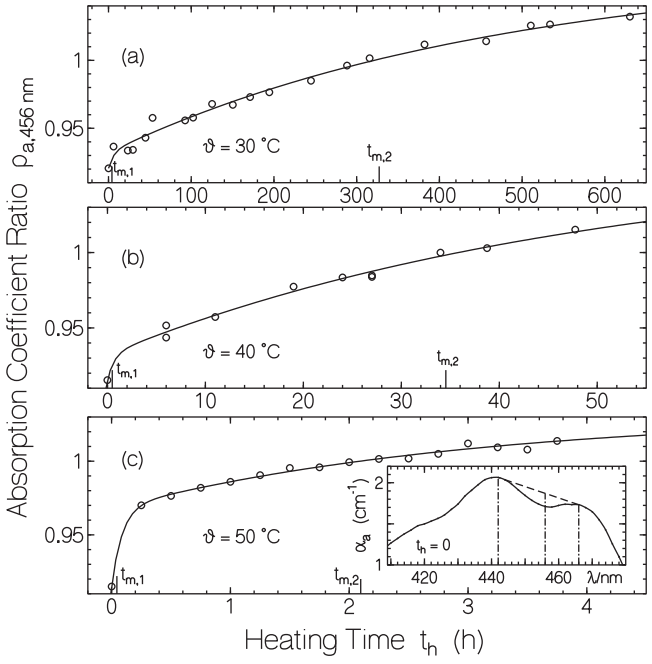

Fig. 6. Temporal development of nPAC protein unfolding. The absorption coefficient ratio $\rho_{a,456\,nm}$ versus heating time is depicted. The sample temperatures are (a) $\vartheta = 30\,^{\circ}C$, (b) $\vartheta = 40\,^{\circ}C$, and (c) $\vartheta = 50\,^{\circ}C$. The curves are fitted to the data points using Eq. (1). The inset in (c) shows the flavin cofactor absorption coefficient spectrum, $\alpha_a(\lambda)$, before sample heating ($t_h = 0$).

fluorescence excitation spectrum obtained in the case of fluorescence detection at 340 nm is thought belong to the denatured nPAC apo-protein in solution.

3.2. Temperature dependent temporal protein unfolding

The temporal development of the nPAC protein unfolding at selected temperatures was determined from changes of the shape of the S_0–S_1 flavin cofactor absorption band due to flavin release from the BLUF domain binding pocket. The vibronic structure of the first absorption band of non-covalently bound flavin is smeared out by flavin release. The samples were thermostated to fixed temperatures and absorption spectra were recorded periodically. As a parameter of the absorption spectra change the absorption coefficient ratio, $\rho_{a,456\,nm} = \alpha_a(456\,nm)/\alpha_{a,lin}(456\,nm)$ was used, where $\alpha_a(456\,nm)$ is the measured absorption coefficient at 456 nm and $\alpha_{a,lin}(456\,nm)$ is the linear interpolated absorption coefficient at 456 nm using the absorption peaks at 442 nm and 466 nm. This linear interpolated value is given by $\alpha_{a,lin}(456\,nm) = \alpha_a(442\,nm) + [(\alpha_a(466\,nm) - \alpha_a(442\,nm))/(466 - 442)](456 - 442)$.

In Fig. 6 $\rho_{a,456\,nm}$ is displayed versus heating time t_h for the sample temperatures $\vartheta = 30\,^{\circ}C$ (a), $40\,^{\circ}C$ (b), and $50\,^{\circ}C$ (c). The inset in Fig. 6c shows part of the S_0–S_1 absorption spectrum of flavin in nPAC at $t_h = 0$ to illustrate $\alpha_a(456\,nm)$, $\alpha_a(442\,nm)$, $\alpha_a(466\,nm)$, and $\alpha_{a,lin}(456\,nm)$. The curves in Fig. 6a–c are nonlinear regression fits to the experimental points using the functional dependence

$$\rho_{a,456\,nm}(t_h) = \rho_{a,456\,nm}(0) + \Delta\rho_{a,456\,nm}\left\{x_1\left[1 - \exp\left(\frac{-t_h}{\tau_{m,1}}\right)\right] + x_2\left[1 - \exp\left(\frac{-t_h}{\tau_{m,2}}\right)\right]\right\} \quad (1)$$

where $\rho_{a,456\,nm}(0)$ is the absorption coefficient ratio of the unheated sample (protein folded), $\Delta\rho_{a,456\,nm} = \rho_{a,456\,nm}(\infty) - \rho_{a,456\,nm}(0)$ is the difference in the absorption coefficient ratio between the heated sample at $t_h = \infty$ (protein unfolded) and the unheated sample at $t_h = 0$ (protein folded), x_1 is the mole-fraction of nPAC protein molecules which unfold quickly with melting time constant $\tau_{m,1}$ (nPAC molecules forming the surface of the nPAC nano-clusters), and x_2 is the mole-fraction of nPAC protein molecules which unfold slowly with melting time constant $\tau_{m,2}$ (nPAC molecules forming the interior of the nPAC nano-clusters). The corresponding melting half-times are $t_{m,1} = \ln(2)\tau_{m,1}$, and $t_{m,2} = \ln(2)\tau_{m,2}$. The obtained melting times are $t_{m,1}(30\,^{\circ}C) = 4.2 \pm 1.4\,h$, $t_{m,2}(30\,^{\circ}C) = 330 \pm 40\,h$, $t_{m,1}(40\,^{\circ}C) = 0.5 \pm 0.2\,h$, $t_{m,2}(40\,^{\circ}C) = 34.5 \pm 5\,h$, $t_{m,1}(50\,^{\circ}C) = 3.7 \pm 1\,min$, and $t_{m,2}(50\,^{\circ}C) = 2.1 \pm 0.4\,h$. The $\pm$ values are estimated uncertainties of the fitted $t_{m,1}$ and $t_{m,2}$ values.

The experimental melting times, $t_{m,1}$ and $t_{m,2}$, as a function of temperature, ϑ, are shown in Fig. 7a as circles and dots. An exponential rise of $t_{m,1}$ and $t_{m,2}$ with decreasing ϑ is observed. A description of the temperature dependence of the melting times is developed in the discussion part and the theoretical fit curves are determined there.

The two dashed-line connected triangles in Fig. 7a show the time positions, $t_{m,sca}$, of maximum change of light scattering, $\partial\sigma_{sca}(700\,nm)/\partial t|_{max}$, at $\vartheta = 50\,^{\circ}C$ and $60\,^{\circ}C$ due to protein aggregation. They represent the nPAC nano-cluster melting half-times determined by light-scattering studies.

4. Discussion

The applied staircase temperature profile of nPAC heating resulted in fast protein unfolding at about $60\,^{\circ}C$ showing up in strong increase of light scattering due to aggregation (coalescing of nano-clusters), smoothening of the S_0–S_1 flavin absorption band and increase of the flavin fluorescence due to flavin cofactor release. In the following the protein aggregation is described by analysis of the nPAC light scattering, and the kinetics of irreversible protein unfolding is described with a thermal driven transition-state-crossing reaction process. For comparison a short description

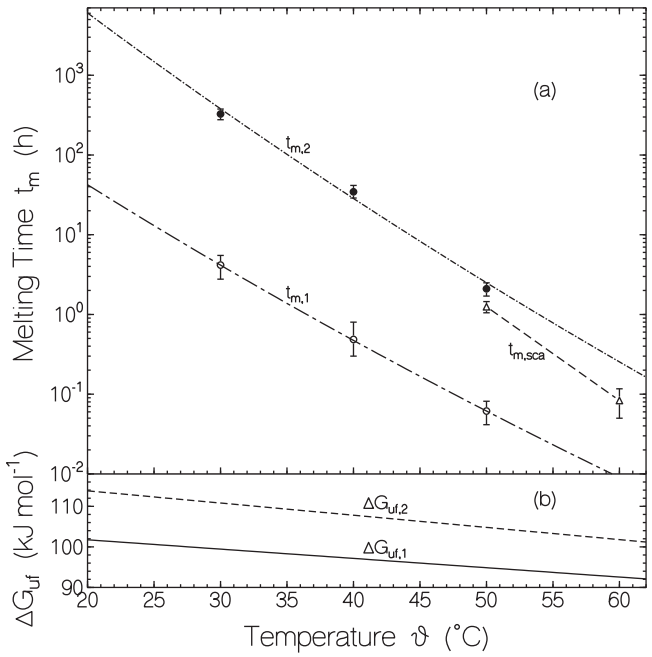

Fig. 7. (a) Melting half-times, t_m, of nPAC nano-clusters in pH 7.5 aqueous solution as a function of temperature, ϑ. Markers show experimental results, curves are calculated fits (Eq. (11)). Circles: melting times, $t_{m,1}$, of nPAC protein molecules at nano-cluster surface. Dots: melting times, $t_{m,2}$, of nPAC protein molecules in nano-cluster interior. Triangles: melting times, $t_{m,sca}$, of nPAC nano-clusters determined by light scattering (time positions of maximum $\partial\sigma_{sca}(700\,nm, t)/\partial t$). (b) Gibbs free energy of protein unfolding ΔG_{uf} for nPAC molecules at nano-cluster surface (solid curve) and in nano-cluster interior (dashed curve).

Table 1
Parameters of nPAC concerning protein unfolding.

Parameter	Value	Comments
M_{pr}	43962 g mol^{-1}	
ρ_{pr}	≈1.412 g cm^{-3}	Typical value [56]
N_{aa}	390	
$V_{m,f}$	≈51.7 nm^3	Eq. (2)
$a_{m,f}$	≈2.31 nm	Eq. (2)
$V_{m,gy,uf}$	≈1678 nm^3	Eq. (3)
$a_{m,gy,uf}$	≈7.35 nm	Eq. (3)
$a_{m,uf}$	≈10.4 nm	$a_{m,uf} = 2^{1/2} a_{m,gy,uf}$
$V_{m,uf}$	≈4750 nm^3	$V_{m,uf} = (4\pi/3) a_{m,uf}^3$
n_{pr}(700 nm)	≈1.587	Typical value [58]
$\sigma_{R,m}$	≈1.77 × 10^{-21} cm^2	Eq. (5b)
ϑ_m	≈60 °C	Fig. (3), heating profile dependent
$t_{m,1}$(20 °C)	≈42 h	Fit curve in Fig. 7a
$t_{m,2}$(20 °C)	≈250 d	Fit curve in Fig. 7a
$\Delta H_{uf,1}$	≈40.4 kcal mol^{-1}	Fig. 7a and fit to Eq. (11)
$\Delta S_{uf,1}$	≈54.88 cal K^{-1} mol^{-1}	Fig. 7a and fit to Eq. (11)
$\Delta H_{uf,2}$	≈48.26 kcal mol^{-1}	Fig. 7a and fit to Eq. (11)
$\Delta S_{uf,2}$	≈71.85 cal K^{-1} mol^{-1}	Fig. 7a and fit to Eq. (11)

Abbreviations: M_{pr}, molar mass of nPAC apo-protein; ρ_{pr}, mass density of protein; N_{aa}, number of amino acids per nPAC protein; $V_{m,f}$, volume of folded nPAC monomer; $a_{m,f}$, radius of folded nPAC monomer; $V_{m,gy,uf}$, gyration volume of unfolded nPAC monomer; $a_{m,gy,uf}$, gyration radius of unfolded nPAC monomer; $a_{m,uf}$, radius of unfolded nPAC monomer; $V_{m,uf}$, volume of unfolded nPAC monomer; n_{pr}, refractive index of protein; $\sigma_{R,m}$, monomeric Rayleigh scattering cross-section of nPAC; ϑ_m, apparent melting temperature of nPAC; $t_{m,1}$, melting time of nPAC molecules at cluster surface; $t_{m,2}$, melting time of nPAC molecules in cluster interior; $\Delta H_{uf,1}$, enthalpy of nPAC protein unfolding at cluster surface; $\Delta S_{uf,1}$, entropy of nPAC protein unfolding at cluster surface; $\Delta H_{uf,2}$, enthalpy of nPAC protein unfolding in cluster interior; $\Delta S_{uf,2}$, entropy of nPAC protein unfolding in cluster interior.

of the thermodynamics of reversible protein unfolding and refolding is included. Some parameters of nPAC involved in the thermal denaturation and determined in the present denaturation studies are collected in Table 1.

4.1. Protein aggregation during melting temperature measurement procedure

The protein unfolding increases the protein size in the change from a tightly packed globule structure to a random coil structure. The volume of a native folded protein monomer molecule is given by

$$V_{m,f} = \left(\frac{4\pi}{3}\right) a_{m,f}^3 = \frac{M_{pr}}{N_A \rho_{pr}} \tag{2}$$

where $a_{m,f}$ is the folded protein monomer radius assuming globular (spherical) shape, M_{pr} is the protein molar mass, N_A is the Avogadro constant, and ρ_{pr} is the protein mass density. The parameters of nPAC are M_{pr} = 43 962 g mol^{-1} (molar mass of cofactor is neglected) and $\rho_{pr} \approx 1.412$ g cm^{-3} (typical value for proteins [57]) giving $V_{m,f} \approx 51.7$ nm^3 and $a_{m,f} \approx 2.31$ nm.

The gyration volume of an unfolded (random coil) nPAC (protein monomer) molecule is given by [42,58]

$$V_{m,gy,uf} = \left(\frac{4\pi}{3}\right) a_{m,gy,uf}^3 \approx \left(\frac{4\pi}{3}\right) (R_0 N_{aa}^{\nu})^3 \tag{3}$$

where $a_{m,gy,uf}$ is the unfolded molecule gyration radius, $R_0 \approx 0.208 \pm 0.019$ nm is a characteristic amino acid length, N_{aa} is the number of amino acids per protein, and $\nu = 0.598 \pm 0.029$ is an exponential scaling factor. nPAC consists of 390 amino acids giving an unfolded gyration radius of $a_{m,gy,uf} = R_0 N_{aa}^{\nu} \approx 7.35$ nm and a gyration volume of $V_{m,gy,uf} \approx 1678$ nm^3. The gyration radius is defined as $a_{m,gy} = (I_m/A_m)^{1/2} = [\int_0^{a_m} r^2 2\pi r dr/(\pi a_m^2)]^{1/2} = 2^{-1/2} a_m$ where I_m is the second moment of area and A_m is the area. The unfolded monomeric nPAC radius is therefore $a_{m,uf} = 2^{1/2} a_{m,gy,uf} \approx 10.4$ nm and the corresponding volume $V_{m,uf} \approx 4750$ nm^3.

The cluster volume of native folded nPAC with degree of aggregation β_m (β_m = average number of proteins per cluster) is

$$V_{ag,f} = \beta_m V_{m,f} \tag{4a}$$

and the cluster radius is

$$a_{ag,f} = \beta_m^{1/3} a_{m,f} \tag{4b}$$

The cluster volume of an unfolded nPAC with sufficiently large degree of aggregation β_m is thought to be

$$V_{ag,uf} \approx \beta_m V_{m,gy,uf} \tag{4c}$$

and the corresponding aggregate radius is thought to be

$$a_{ag,uf} \approx \beta_m^{1/3} a_{m,gy,uf} \tag{4d}$$

In Eqs. (4c) and (4d) the unfolded monomer gyration volume and the unfolded monomer gyration radius are used in an approximate manner for the full unfolded cluster volume and the full unfolded cluster radius instead of the total unfolded monomer volume and radius since the random-coil unfolded proteins are entangled and intermixed lowering their size. In Fig. 8a a folded protein monomer, in Fig. 8b a random-coil unfolded protein monomer, and in Fig. 8c a random-coil unfolded protein aggregate (trimer) are sketched for illustration of the discussed situation.

The scattering cross-section, σ_{sca}, of a single protein molecule in a cluster consisting of β_m protein molecules (β_m is degree of aggregation) is given by [49]

$$\sigma_{sca} = \beta_m \tilde{M} \sigma_{R,m} \tag{5a}$$

with the total Mie scattering function, $\tilde{M}$, and the single monomeric protein molecule Rayleigh scattering cross-section, $\sigma_{R,m}$, ($\sigma_{R,m}$ is the same for folded and unfolded protein) which is given

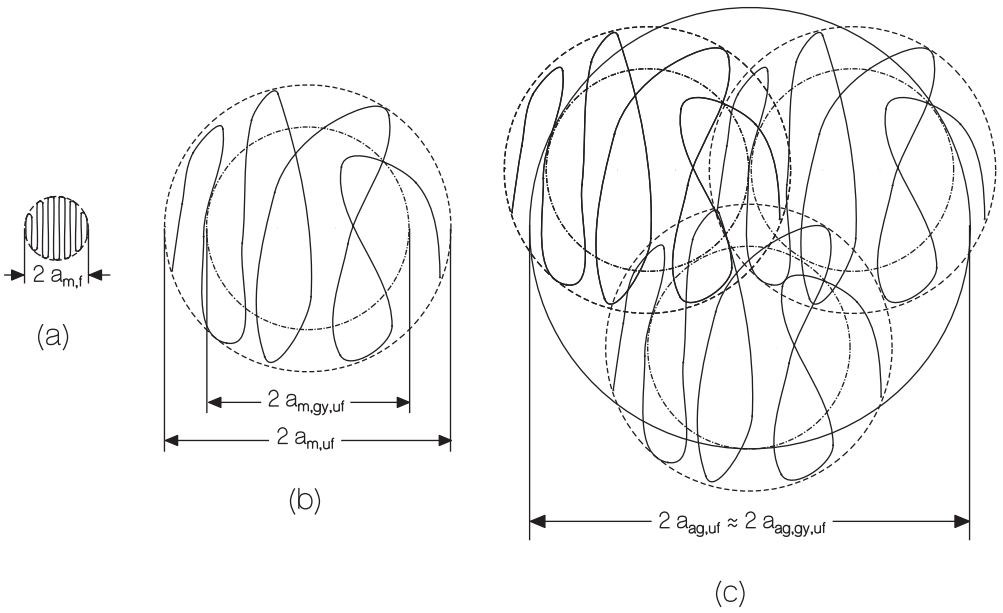

Fig. 8. Illustration of (a) native folded protein monomer, (b) random-coil unfolded protein monomer, and (c) random-coil unfolded protein aggregate (trimer).

by [49]

$$\sigma_{R,m} = \frac{8\pi}{3}\frac{4\pi^2 n_s^4}{\lambda^4}V_{m,f}^2\left(\frac{n_{pr}^2 - n_s^2}{n_{pr}^2 + 2n_s^2}\right)^2 = \frac{8\pi}{3}\frac{4\pi^2 n_s^4}{\lambda^4}\left(\frac{M_{pr}}{N_A\rho_{pr}}\right)^2\left(\frac{n_{pr}^2 - n_s^2}{n_{pr}^2 + 2n_s^2}\right)^2 \quad (5b)$$

Thereby n_s is the refractive index of the solvent (water buffer) at wavelength λ, and n_{pr} the refractive index of the protein at wavelength λ. At $\lambda = 700$ nm (see Figs. 2 and 3) the refractive indices are $n_s = 1.330$ and $n_{pr} \approx 1.587$ [59], and Eq. (5b) gives $\sigma_{R,m} \approx 1.77 \times 10^{-21}$ cm^2 for the monomer Rayleigh scattering cross-section of nPAC in aqueous solution.

The development of the nPAC scattering cross-section σ_{sca} of Fig. 2b is caused by aggregation (increase of β_m) due to coalescing of unfolded protein clusters in the protein melting process. The corresponding development of the aggregation factor, $\beta_m\tilde{M} = \sigma_{sca}/\sigma_{R,m}$, is depicted in Fig. 9a. The *in vitro* native protein aggregation factor is of the order of $\beta_m\tilde{M} \approx 500$. During protein unfolding (protein melting) at $\vartheta_m = 60\,^\circ$C in the time interval from 42 min to 50 min the aggregation factor increased up to $\beta_m\tilde{M} \approx 26\,300$. In heating up to 90 °C ($t = 110$ min) the aggregation factor increased to $\beta_m\tilde{M} \approx 37\,000$. In the cooling down process to 20 °C the aggregation slowly continued to increase to $\beta_m\tilde{M} \approx 39,000$ ($t = 210$ min).

The total Mie scattering function $\tilde{M}$ decreases with aggregate radius (destructive interference reduces light scattering). The dependence of $\tilde{M}$ on the aggregate (cluster) radius a_{ag} is shown by the solid curve in Fig. 10. The functional dependence of $\tilde{M}(a_{ag})$ is given in [49] (Eq.(16) there). The aggregate volume, V_{ag}, increases with the degree of aggregation according to $V_{ag} = (4\pi/3)a_{ag}^3 = \beta_m V_m = \beta_m(4\pi/3)a_m^3$. For the folded protein it is $\beta_{m,f} = (a_{ag}/a_{m,f})^3$, and for the unfolded (random coil) protein it is $\beta_{m,uf} = (a_{ag}/a_{m,gy,uf})^3$. These degrees of aggregation of folded and unfolded nPAC versus cluster radius a_{ag} are included in Fig. 10.

The dependence of $\tilde{M}$ on the aggregation factor, $\beta_m\tilde{M} = \sigma_{sca}/\sigma_{R,m}$, for the folded nPAC and the unfolded nPAC is shown in Fig. 11a. It is obtained by re-plotting of $\tilde{M}(r_{ag})$, $\beta_{m,f}(r_{ag})$, and $\beta_{m,uf}(r_{ag})$ from Fig. 10. In Fig. 11b the degrees of aggregation, $\beta_{m,f}$ and $\beta_{m,uf}$, of nPAC versus the aggregation factor, $\beta_m\tilde{M} = \sigma_{sca}/\sigma_{R,m}$, are shown. At a fixed value of $\sigma_{sca}/\sigma_{R,m}$ the corresponding degree of aggregation of unfolded nPAC is larger than of folded nPAC since the aggregate size of the unfolded protein is larger and therefore $\tilde{M}$ smaller (more effective destructive interference).

Knowing the dependence of $\beta_m(\beta_m\tilde{M}) = \beta_m(\sigma_{sca}/\sigma_{R,m})$ from Fig. 11b the dependence of development of β_m in the nPAC thermal unfolding process gets accessible from Figs. 9a and 11b. It is depicted in Fig. 9b. In the heating process up to 90 °C and the cooling process back to room temperature the degree of aggregation increased from initial $\beta_{m,f} \approx 500$ to final $\beta_{m,uf} \approx 8 \times 10^6$. The average nPAC cluster size increased from $V_{ag,f} = \beta_{m,f}V_{m,f} \approx 2.6 \times 10^4$ nm^3 ($a_{ag,f} \approx 18.3$ nm) at the beginning to $V_{ag,uf} = \beta_{m,uf}V_{m,gy,uf} \approx 13.4\,\mu$m^3 ($a_{ag,uf} \approx 1.47\,\mu$m) at the end.

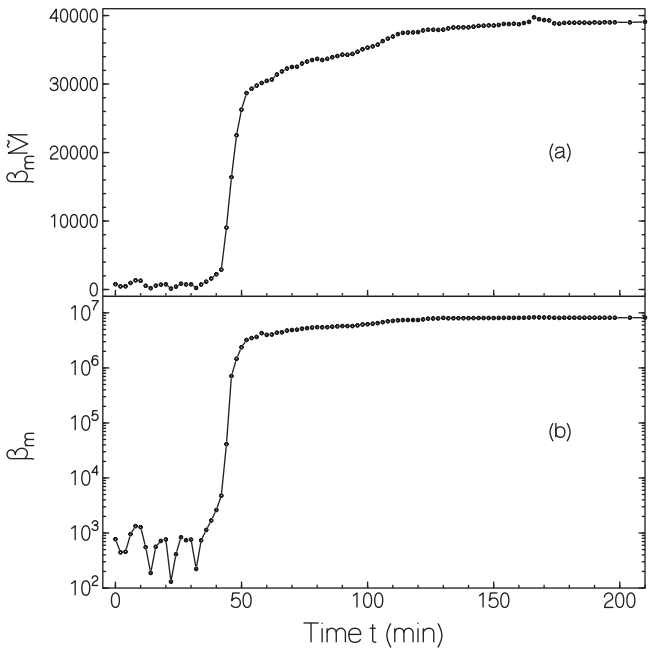

Fig. 9. Development of (a) aggregation factor, $\beta_m\tilde{M} = \sigma_{sca}/\sigma_{R,m}$, and (b) of degree of aggregation (number of protein molecules in cluster), β_m, versus time for temperature profile of Fig. 2a.

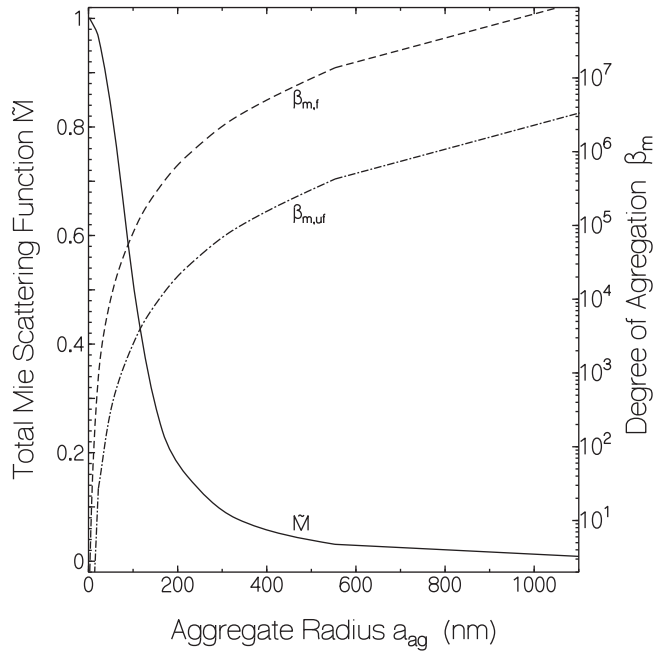

Fig. 10. Dependence of total Mie scattering function $\tilde{M}$ (solid curve), of degree of aggregation $\beta_{m,f}$ of folded nPAC (dashed curve), and of degree of aggregation $\beta_{m,uf}$ of unfolded nPAC (dash-dotted curve) on the aggregate (cluster) radius a_{ag}. The $\tilde{M}$ curve applies to wavelength of $\lambda = 700$ nm and solvent refractive index of $n_s = 1.330$.

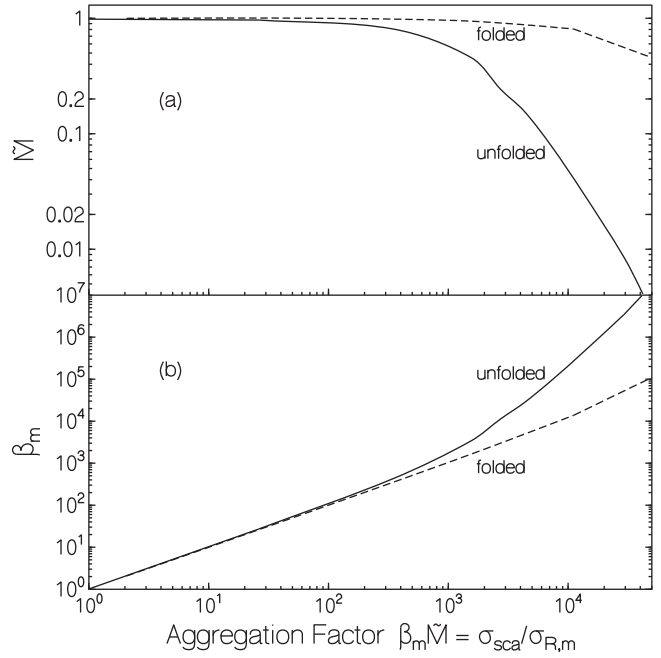

Fig. 11. Total Mie scattering function $\tilde{M}$ (a) and degree of aggregation β_m (b) for folded nPAC (dashed curves) and unfolded nPAC (solid curves) as a function of the aggregation factor $\beta_m\tilde{M} = \sigma_{sca}/\sigma_{R,m}$ at wavelength of $\lambda = 700$ nm.

4.2. Thermodynamics of reversible protein unfolding

In the case of reversible protein unfolding under steady-state conditions there exists a thermodynamic equilibrium between the folded native state N and the unfolded state U [15,28,32–34,36,40] according to the equilibrium reaction

$$N \underset{k_f}{\overset{k_{uf}}{\rightleftharpoons}} U \tag{R1}$$

with the N and U number density relation

$$\frac{dN}{dt} = -k_{uf}N + k_f U = -\frac{dU}{dt} = 0 \tag{6}$$

giving the unfolding equilibrium constant

$$K_{uf} = \frac{U}{N} = \frac{k_{uf}}{k_f} = \exp\left(-\frac{\Delta G_{uf}}{N_A k_B \vartheta}\right) = \exp\left(-\frac{\Delta H_{uf} - \vartheta \Delta S_{uf}}{N_A k_B \vartheta}\right) = \frac{f_{uf}}{1 - f_{uf}} \tag{7}$$

k_{uf} is the uni-molecular rate-constant of protein unfolding, and k_f is the uni-molecular rate-constant of protein refolding. f_{uf} is the mole-fraction of unfolded proteins, and $f_f = 1 - f_{uf}$ is the mole-fraction of folded proteins. ΔG_{uf} is the Gibbs free energy, ΔH_{uf} the enthalpy, and ΔS_{uf} the entropy of protein unfolding. N_A is the Avogadro constant, k_B is the Boltzmann constant, and ϑ is the temperature in Kelvin. The protein melting temperature, ϑ_m, is defined by the condition $K_{uf} = [U]/[N] = 1$, which implies $\Delta G_{uf} = 0$ and $\vartheta_m = \Delta H_{uf}/\Delta S_{uf}$ [34,60].

Reversible protein unfolding rarely occurs [9,17–19]. It may be observed when the proteins are present in monomeric folded form in the solution under investigation. In this case only very weak monomeric protein Rayleigh scattering takes place and does not change by unfolding of the protein. The speed of steady-state formation is protein and solvent dependent and increases with rising temperature. Correspondingly the time duration of steady state formation depends on the special protein and decreases with rising temperature.

4.3. Dynamics of irreversible protein unfolding

In our case, the native folded nPAC in aqueous solution at pH 7.5 was packed to nano-crystallites/nano-clusters. The thermal protein unfolding in the nano-clusters to random-coils entangled the individual random-coil protein molecules in the clusters to an intermixed random-coil cluster which was not able to disentangle to folded protein molecules packed in nano-crystallites/nano-clusters by decreasing the temperature. The thermal protein unfolding in the protein melting process was irreversible. The protein molecule unfolding started at the nano-cluster surface with faster rate due to free space to expand and due to interaction with the solvent, and it evolved to the interior with slower rate. The clusters of unfolded nPAC coalesced to larger clusters of micrometer size.

The dynamics of irreversible protein unfolding may be described by the reaction [36]

$$N_i \xrightarrow{K_{uf,i}} U_i \tag{R2}$$

where the index $i = 1$ stands for surface nPAC molecules and $i = 2$ stands for interior nPAC molecules. The time derivatives of the number densities, N_i, of native folded protein is given by

$$\frac{dN_i}{dt} = -k_{uf,i}N_i \tag{8}$$

The solution of Eq. (8) is:

$$N_i(t) = N_0 x_i \ \exp(-k_{uf,i}t) = N_0 x_i \ \exp\left(\frac{-t}{\tau_{uf,i}}\right) \tag{9}$$

where x_1 is the fraction of nPAC molecules at the nano-cluster surface, x_2 is the fraction of nPAC molecules at the nano-cluster interior. $k_{uf,i}$ are the rate constants of protein unfolding, and $\tau_{uf,i}$

are the time constants of protein unfolding. The rate constants of protein unfolding are approximately given by

$$k_{\mathrm{uf},i} = k_0\, exp\left(-\frac{\Delta G_{\mathrm{uf},i}}{N_\mathrm{A} k_\mathrm{B} \vartheta}\right) \approx \frac{k_\mathrm{B}\vartheta}{h} \exp\left(-\frac{\Delta H_{\mathrm{uf},i} - \vartheta \Delta S_{\mathrm{uf},i}}{N_\mathrm{A} k_\mathrm{B} \vartheta}\right) \quad (10)$$

where h is the Planck constant, k_B is the Boltzmann constant, and k_0 is the pre-exponential factor. In Eq. (10) the relation $k_0 \approx k_\mathrm{B}\vartheta/h$ ($=6.1\times10^{12}\,\mathrm{s}^{-1}$ at $\vartheta = 293\,\mathrm{K}$) is used for the pre-exponential factor (attempt frequency of transition state barrier crossing) of the Arrhenius type relation of transition state crossing [61]. $k_0 h$ is the average energy of the vibration that leads to the unfolding at the transition state. This energy at temperature ϑ is the thermal energy $k_\mathrm{B}\vartheta$ of the transition state crossing vibrational mode. It should be noted the Gibbs free energy $\Delta G_{\mathrm{uf},i}$ depends only slightly (logarithmically) on the pre-exponential factor.

The rate constant of unfolding of protein species i is related to the melting time or half-life, $t_{\mathrm{m},i}$ [60] of unfolding 50% of protein species i by (see Eq. (9))

$$t_{\mathrm{m},i} = \frac{\ln(2)}{k_{\mathrm{uf},i}} = \ln(2)\tau_{\mathrm{uf},i} \approx \frac{h\ln(2)}{k_\mathrm{B}\vartheta} \exp\left(\frac{\Delta H_{\mathrm{uf},i} - \vartheta\Delta S_{\mathrm{uf},i}}{N_\mathrm{A} k_\mathrm{B}\vartheta}\right) \quad (11)$$

In the experiments $t_{\mathrm{m,i}}$ was determined (see Fig. 7a). A fit of Eq. (11) to the experimental melting times $t_{\mathrm{m},i}(\vartheta)$ gives values for the enthalpy $\Delta H_{\mathrm{uf},i}$ and the entropy $\Delta S_{\mathrm{uf},i}$ of protein unfolding. Analytical formulae for the thermodynamic parameters, $\Delta H_{\mathrm{uf},i}$ and $\Delta S_{\mathrm{uf},i}$, are

$$\Delta H_{\mathrm{uf},i} = \frac{\vartheta_1\vartheta_2}{\vartheta_1 - \vartheta_2} N_\mathrm{A} k_\mathrm{B} \ln\left(\frac{t_{\mathrm{m},i}(\vartheta_2)\vartheta_2}{t_{\mathrm{m},i}(\vartheta_1)\vartheta_1}\right) \quad (12a)$$

$$\Delta S_{\mathrm{uf},i} = \frac{N_\mathrm{A} k_\mathrm{B}}{\vartheta_1 - \vartheta_2}\left[\vartheta_1 \ln\left(\frac{h}{k_\mathrm{B}\vartheta_1 t_{\mathrm{m},i}(\vartheta_1)}\right) - \vartheta_2 \ln\left(\frac{h}{k_\mathrm{B}\vartheta_2 t_{\mathrm{m},i}(\vartheta_2)}\right)\right] \quad (12b)$$

The best fitting enthalpy and entropy values to the temperature dependence of the melting times in Fig. 7a are $\Delta H_{\mathrm{uf},1} \approx 169.09\,\mathrm{kJ\,mol^{-1}}$ ($40.4\,\mathrm{kcal\,mol^{-1}}$) and $\Delta S_{\mathrm{uf},1} \approx 229.73\,\mathrm{J\,K^{-1}\,mol^{-1}}$ ($54.88\,\mathrm{cal\,mol^{-1}}$) for nPAC melting at the nano-cluster surface, and $\Delta H_{\mathrm{uf},2} \approx 202\,\mathrm{kJ\,mol^{-1}}$ ($48.26\,\mathrm{kcal\,mol^{-1}}$) and $\Delta S_{\mathrm{uf},2} \approx 300.75\,\mathrm{J\,K^{-1}\,mol^{-1}}$ ($71.85\,\mathrm{cal\,mol^{-1}}$) for nPAC melting in the nano-cluster interior. The functions $\Delta G_{\mathrm{uf},1}(\vartheta)$ and $\Delta G_{\mathrm{uf},2}(\vartheta)$ for nPAC are shown in Fig. 7b.

The nano-crystallite/nano-cluster form of thawed nPAC gives these proteins a very high thermal stability. As seen from the curves in Fig. 7a at 20 °C the nPAC molecule unfolding at the cluster surface has a half-time of $t_{\mathrm{m},1} \approx 42\,\mathrm{h}$ while the complete protein unfolding in the cluster has a half-time of $t_{\mathrm{m},2} \approx 6000\,\mathrm{h} = 250\,\mathrm{d}$. The BLUF domain photo-cycle dynamics of nPAC could be conveniently studied at room temperature in [7] because of the slow nPAC protein melting time in the nano-clusters.

5. Conclusions

The thermal protein unfolding of nPAC in aqueous solution at pH 7.5 was studied by stepwise sample heating and recording of transmission spectra (steps of 10 °C every 10 min in intervals of small transmission changes and steps of 5 °C every 10 min in intervals of strong transmission change). The light attenuation in the non-absorption region of the protein was applied for the determination of the apparent protein melting temperature ϑ_m.

Since nPAC dissolved only to oligomeric nano-clusters the protein unfolding occurred in an irreversible manner and the time constant of nPAC unfolding at the cluster surface was shorter than in the cluster interior. The nano-clustering made nPAC thermally very stable. The unfolded random-coil-like nano-clusters coalesced to micro-clusters with strong increase of light scattering. In the denaturation (unfolding) process the flavin cofactor of nPAC was released from its binding pocket with strong increase of fluorescence emission.

While for reversible unfolding proteins a melting temperature, ϑ_m, is well defined by the temperature where under steady-state conditions the fraction of unfolded proteins is 50% (there the rates of unfolding and refolding are equal), this is not the case for irreversible unfolding proteins. For irreversible unfolding proteins only an apparent melting temperature is measurable which depends on the applied temperature heating profile. In this paper a heating and cooling temperature profile has been applied and the protein denaturation was followed by light attenuation measurements. The applied measurement scheme may be applied as a general measurement standard of melting temperature determination of irreversible denaturating proteins or DNA samples.

Acknowledgements

The authors thank the Deutsche Forschungsgemeinschaft (DFG) for support of the research group FOR 526 “Sensory Blue Light Receptors”, which enabled this collaborative work. We are thankful to BMBF, Germany, and DBT, India for financial support of the joint Indo-German project. A.P. thanks Prof. F.J. Gießibl for his kind hospitality.

References

[1] J.F. De Jonckheere, A century of research on the amoeboflagellate genus *Naegleria*, Acta Protozool. 41 (2002) 309–342.
[2] C. Fulton, Axenic cultivation of *Naegleria gruberi*. Requirement for methionine, Exp. Cell Res. 88 (1974) 365–370.
[3] C. Fulton, C. Webster, J.S. Wu, Chemically defined media for cultivation of *Naegleria gruberi*, PNAS 81 (1984) 2406–2410.
[4] C. Fulton, *Naegleria*: a research partner for cell and developmental biology, J. Eukaryot. Microbiol. 40 (1983) 520–532.
[5] L.K. Fritz-Laylin, S.E. Prochnik, M.L. Ginger, J.B. Dacks, M.L. Carpenter, M.C. Field, A. Kuo, A. Paredez, J. Chapman, J. Pham, S. Shu, R. Neupane, M. Cipriano, J. Mancuso, H. Tu, A. Salamov, E. Lindquist, H. Shapiro, S. Lucas, I.V. Grigoriev, W.Z. Cande, C. Fulton, D.S. Rokhsar, S.C. Dawson, The genome of *Naegleria gruberi* illuminates early eukaryotic versatility, Cell 140 (2010) 631–642.
[6] J.U. Linder, J.E. Schultz, The class III adenylyl cyclases: multi-purpose signalling modules, Cell. Signal. 15 (2003) 1081–1089.
[7] A. Penzkofer, M. Stierl, P. Hegemann, S. Kateriya, Photo-dynamics of the BLUF domain containing soluble adenylate cyclase (nPAC) from the amoeboflagellate *Naegleria gruberi* NEG-M strain, Chem. Phys. 387 (2011) 25–38.
[8] A. Penzkofer, M. Stierl, P. Hegemann, S. Kateriya, Absorption and fluorescence characteristics of photo-activated adenylate cyclase nano-clusters from the amoeboflagellate *Naegleria gruberi* NEG-M strain, Chem. Phys., (2011) doi:10.1016/j.chemphys.2011.09.005.
[9] P.L. Privalov, Stability of proteins. Small globular proteins, Adv. Protein Chem. 33 (1979) 167–241.
[10] J. Walters, S.L. Milam, A.C. Clark, Practical approaches to protein folding and assembly: spectroscopic strategies in thermodynamics and kinetics, Methods Enzymol. 455 (2009) 1–39.
[11] W. Kauzmann, Some factors in the interpretation of protein denaturation, Adv. Protein Chem. 14 (1959) 1–63.
[12] P.L. Privalov, S.J. Gill, Stability of protein structure and hydrophobic interaction, Adv. Protein Chem. 33 (1988) 191–234.
[13] L.M. Gloss, Equilibrium and kinetic approaches for studying oligomeric protein folding, Methods Enzymol. 466 (2009) 325–357.
[14] E.A. Franzosa, K.J. Lynagh, Y. Xia, Structural correlates of protein melting temperature, http://www.beilstein-institute.de/ESCEC2009/Proceedings/Xia/Xia.pdf.
[15] M.R. Eftink, The use of fluorescence methods to monitor unfolding transitions in proteins, Biophys. J. 66 (1994) 482–501.
[16] S.C. Fujita, N. Gō, K. Imahori, Melting-profile analysis of thermal stability of thermolysin. A formulation of temperature-scanning kinetics, Biochemistry 18 (1979) 24–28.
[17] P. Alexander, S. Fahnestock, T. Lee, J. Orban, P. Bryan, Thermodynamic analysis of the folding of the streptococcal protein G IgG-binding domains B1 and B2: why small proteins tend to have high denaturation temperatures, Biochemistry 31 (1992) 3597–3603.

[18] I.V. Sochava, T.V. Belopolskaya, O.I. Smirnova, DSC study of reversible and irreversible thermal denaturation of concentrated globular protein solutions, Biophys. Chem. 22 (1985) 323–336.
[19] B.S. McCrary, S.P. Edmondson, J.W. Shriver, Hyperthermophile protein folding thermodynamics: differential scanning calorimetry and chemical denaturation of Sac7d, J. Mol. Biol. 264 (1996) 784–805.
[20] J.M. Andreu, M.A. Oliva, O. Monasterio, Reversible unfolding of FtsZ cell division proteins from archaea and bacteria, J. Biol. Chem. 277 (2002) 43262–43270.
[21] J.A. Schellman, Fifty years of solvent denaturation, Biophys. Chem. 96 (2002) 91–101.
[22] E.A. Roman, J.M. Argüello, F.L.G. Flecha, Reversible unfolding of a thermophilic membrane protein in phospholipid/detergent mixed micelles, J. Mol. Biol. 397 (2010) 550–559.
[23] S. Cavagnero, Z.H. Zhou, M.W.W. Adams, S.I. Chan, Response of rubredoxin from *Pyrococcus furiosus* to environmental changes: implications for the origin of hyperthermostability, Biochemistry 34 (1995) 9865–9873.
[24] R. Hiller, Z.H. Zhou, M.W.W. Adams, S.W. Englander, Stability and dynamics in a hyperthermophilic protein with melting temperature close to 200 °C, PNAS 94 (1997) 11329–11332.
[25] A. Ginsburg, W.R. Carroll, Some specific ion effects on the conformation and thermal stability of ribonuclease, Biochemistry 4 (1965) 2159–2174.
[26] P.H. Hippel, K.Y. Wong, On the conformational stability of globular proteins, J. Biol. Chem. 240 (1965) 3909–3923.
[27] D. Voet, W.B. Gratzer, R.A. Cox, P. Doty, Absorption spectra of nucleotides, polynucleotides, and nucleic acids in the far ultraviolet, Biopolymers 1 (1963) 193–208.
[28] J.R. Lepock, A.M. Rodahl, C. Zhang, M.L. Heynen, B. Waters, K.-H. Cheng, Thermal denaturation of the Ca^{2+}-ATPase of Sarcoplasmic reticulum reveals two thermodynamically independent domains, Biochemistry 29 (1990) 681–689.
[29] Application note, Characterization of protein melting point, Zetasizer nano application note, MRK507-O1, Malvern Instruments Limited, www.malvern.co.uk.
[30] T. Coviello, K. Kajiwara, W. Burchard, M. Dentini, V. Crescenzi, Solution properties of xanthan. Dynamic and static light scattering from native and modified xanthans in dilute solutions, Macromolecules 19 (1986) 2826–2831.
[31] B.I. Kurganov, Kinetics of protein aggregation. Quantitative estimation of the chaperone-like activity in test-systems based on suppression of protein aggregation, Biochemistry (Moscow) 67 (2002) 409–422.
[32] P.L. Privalov, Thermodynamics problems of protein structure, Annu. Rev. Biophys. Biophys. Chem. 18 (1989) 47–69.
[33] K.A. Dill, D.O.V. Alonso, K. Hutchinson, Thermal stabilities of globular proteins, Biochemistry 28 (1989) 5439–5449.
[34] W.J. Becktel, J.A. Schellman, Protein stability curves, Biopolymers 26 (1987) 1859–1877.
[35] A. Nicholls, K.A. Sharp, B. Honig, Protein folding and association: insights from interfacial and thermodynamic properties of hydrocarbons, Protein Struct. Funct. Genet. 11 (1991) 281–296.
[36] J.R. Lepock, K.P. Ritchie, M.C. Kolios, A.M. Rodahl, K.A. Heinz, J. Kruuv, Influence of transition rates and scan rate on kinetic simulations of differential scanning calorimetry profiles of reversible and irreversible protein denaturation, Biochemistry 31 (1992) 12706–12712.
[37] M. Gorania, H. Seker, Pl. Haris, Predicting a protein's melting temperature from its amino acid sequence, Conf. Proc. IEEE Eng. Med. Soc. 1 (2010) 1820–1823.
[38] P.K. Ponnuswamy, R. Muthusamy, P. Manavalan, Amino acid composition and thermal stability of proteins, Int. J. Biol. Macromol. 4 (1982) 186–190.
[39] T. Ku, P. Lu, C. Chan, T. Wang, S. Lai, P. Lyu, N. Hsiao, Predicting melting temperature directly from protein sequences, Comput. Biol. Chem. 33 (2009) 45–450.
[40] D. Shortle, The denatured state (the other half of the folding equation) and its role in protein stability, FASEB J. 10 (1996) 27–34.
[41] D. Shortle, M.S. Ackerman, Persistence of native-like topology in a denatured protein in 8 M urea, Science 293 (2001) 487–489.
[42] N.C. Fitzkee, G.D. Rose, Reassessing random-coil statistics in unfolded proteins, PNAS 101 (2004) 12497–12502.
[43] B. Zagrovic, C.D. Snow, S. Khaliq, M.R. Shirts, V.S. Pande, Native-like mean structure in the unfolded ensemble of small proteins, J. Mol. Biol. 323 (2002) 153–164.
[44] S. Ohnishi, A.L.M. Lee, H. Edgell, D. Shortle, Direct demonstration of structural similarity between native and denatured eglin C, Biochemistry 43 (2004) 4064–4070.
[45] M.A.C. Reed, C. Jelinska, K. Syson, M.J. Cliff, A. Splevins, T. Alizadeh, A.M. Hounslow, R.A. Staniforth, A.R. Clarke, C.J. Craven, J.P. Waltho, The denatured state under native conditions: a non-native-like collapsed state of N-PGK, J. Mol. Biol. 357 (2006) 365–372.
[46] F. Dörr, Spectroscopy with polarized light, Angew. Chem. Int. Ed. 5 (1966) 478–495.
[47] W. Holzer, M. Pichlmaier, A. Penzkofer, D.D.C. Bradley, W.J. Blau, Fluorescence spectroscopic behaviour of neat and blended conjugated polymer thin films, Chem. Phys. 246 (1999) 445–462.
[48] C. Birkmann, A. Penzkofer, T. Tsuboi, Fluorescence excitation spectroscopic characterisation of colour centres in a LiF crystal, Appl. Phys. B 77 (2003) 625–632.
[49] A. Penzkofer, J. Shirdel, P. Zirak, H. Breitkreuz, E. Wolf, Protein aggregation studied by forward light scattering and light transmission measurement, Chem. Phys. 342 (2007) 55–63.
[50] H.C. van de Hulst, Light Scattering by Small Particles, John Wiley and Sons, New York, 1957.
[51] M. Kerker, The Scattering of Light and other Electromagnetic Radiation, Academic Press, New York, 1969.
[52] W. Holzer, J. Shirdel, P. Zirak, A. Penzkofer, P. Hegemann, R. Deutzmann, E. Hochmuth, Photo-induced degradation of some flavins in aqueous solution, Chem. Phys. 308 (2005) 69–78.
[53] Th. Förster, Fluoreszenz organischer Verbindungen, Vandenhoeck und Ruprecht, Göttingen, 1951.
[54] A. Penzkofer, W. Leupacher, Fluorescence behaviour of highly concentrated rhodamine 6G solutions, J. Lumin. 37 (1987) 61–72.
[55] S.D.M. Islam, T. Susdorf, A. Penzkofer, P. Hegemann, Fluorescence quenching of flavin adenine dinucleotide in aqueous solution by pH dependent isomerisation and photo-induced electron transfer, Chem. Phys. 295 (2003) 139–151.
[56] A. Tyagi, A. Penzkofer, Absorption and emission spectroscopic characterization of lumichrome in aqueous solutions, Photochem. Photobiol. 87 (2011) 524–533.
[57] H. Fischer, I. Polikarpov, A. Craievich, Average protein density is a molecular-weight-dependent function, Protein Sci. 13 (2004) 2825–2828.
[58] J.E. Kohn, I.S. Millett, J. Jacob, B. Zagrovic, T.M. Dillon, N. Cingel, R.S. Dothager, S. Seifert, P. Thiyagarajan, T.R. Sosnick, M.Z. Hasan, V.S. Pande, I. Ruszinski, S. Doniach, K.W. Plaxco, Random-coil behavior and the dimensions of chemically unfolded proteins, PNAS 101 (2004) 12491–12496.
[59] R. Barer, S. Tkaczyk, Refractive index of concentrated protein solutions, Nature 173 (1954) 821–822.
[60] C. Vieille, G.J. Zeikus, Hyperthermophilic enzymes: sources, uses, and molecular mechanisms for thermostabilty, Microbiol. Mol. Biol. Rev. 65 (2001) 1–43.
[61] D. Voet, J.G. Voet, Biochemistry, 3rd ed., John Wiley & Sons, USA, 2004 (Chapter 14).